High Power Laser Science and Engineering, (2018), Vol. 6, e6, 5 pages.
© The Author(s) 2018. This is an Open Access article, distributed under the terms of the Creative Commons Attribution licence (http://creativecommons.org/licenses/by/4.0/), which permits unrestricted re-use, distribution, and reproduction in any medium, provided the original work is properly cited.
doi:10.1017/hpl.2018.1

Directly writing binary multi-sector phase plates on fused silica using femtosecond laser

Li Zhou, Youen Jiang, Peng Zhang, Wei Fan, and Xuechun Li

Shanghai Institute of Optics and Fine Mechanics, Chinese Academy of Sciences, Shanghai 201800, China

(Received 29 September 2017; revised 2 December 2017; accepted 3 January 2018)

Abstract

Light carrying orbital angular momentum (OAM) has a spatial distribution of intensity and phase, which attracts considerable interest regarding several potential applications in optical and quantum scenarios recently. Spiral phase plates are commonly used elements for generating and analyzing OAM states. In this study, we put forward a method of directly writing binary multi-sector phase plates using the femtosecond laser. These phase plates are engraved on fused silica, which could be applied in high-intensity regimes. Different binary multi-sector phase plates were generated with high quality, which were proved by the observation of their structures, accompanied by detecting the beam patterns with the Gaussian beams. The proposed method provides a crucial basis for the rapid manufacturing of phase plates using convenient equipment, which can generate the superposition OAM states and may lead to the capability of measuring the high-dimensional entanglement.

Keywords: femtosecond laser and applications; optical fabrication; phase plate; orbital angular momentum modes

1. Introduction

Orbital angular momentum (OAM) represents a new and fundamental degree of freedom (DOF) of light. Unlike spin angular momentum, which is associated with polarization, the OAM of light contains more abundant and complex information, leading to several applications. Since Allen *et al.*[1] found that a photon of a Laguerre–Gaussian laser mode has a well-defined OAM value in 1992, it has given rise to many developments in optical manipulation[2–4], high-precision optical measurement[5], remote sensing[6–12], and high-capacity communication[13, 14]. Among these applications, higher intensity OAM modes will be more helpful for signal detection, especially for remote sensing[7]. In recent years, OAM has also been introduced into the quantum regime, particularly for the high-dimensional entanglement in OAM DOF[15]. With increasing dimensionality, the OAM entanglement state enables practical applications in photonic dense coding[16, 17], security enhancement against eavesdropping[18, 19], and quantum logic simplification in quantum computation[20].

To generate or analyze the OAM state or OAM superposition state, liquid-crystal spatial light modulators (LC-SLMs)[21–23] and digital micro-mirror device (DMD)[24–29] are typically used for real-time and dynamic operation. However, LC-SLM is costly and can only be used in cases of low power because of their low laser-induced damage threshold, and they have the inconvenience of large sizes and high losses. DMD only has the ability of binary control of amplitude. A typical approach to overcome such limitations involves utilizing of a spiral phase plate (SPP) to convert Gaussian modes into pure OAM modes[30, 31] and a rotatable multi-sector phase plate to produce superposition states[32]. Moreover, multi-sector phase plates with specific patterns have been found to be remarkable candidates for maximizing the Shannon dimensionality D of an entanglement state by selective projective measurements[32, 33]. There have been a multitude of studies regarding the manufacture of these phase plates, including molding techniques[34], e-beam lithography[35], e-beam deposition[36], and direct laser writing by femtosecond laser pulses[37–40]. Utilizing femtosecond laser, Wang *et al.*[39, 40] fabricated microscale geometric phase optical elements from photoresist materials. These phase plates manufactured by femtosecond laser were made from polymer or resist covered on the glass substrate, of which the laser-induced damage thresholds were too low to be used for high-power applications. Utilizing e-beam deposition, a multilevel SPP of 16 steps was developed by SiO_2 vapor deposition using four different types of masks[36], allowing usage in high-intensity laser pulses; however, this is intricate and requires a long period of time for mask fabrication and the deposition procedure.

Correspondence to: L. Zhou, 390 Qinghe Road, Jiading, Shanghai 201800, China. Email: zhoul@siom.ac.cn

https://doi.org/10.1017/hpl.2018.1 Published online by Cambridge University Press

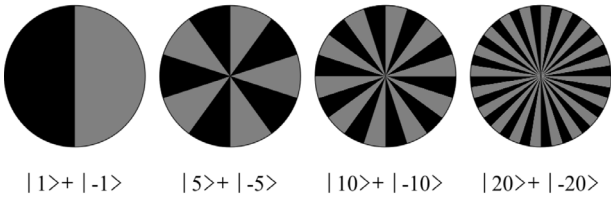

Figure 1. Phase patterns for the OAM superposition states. The black and gray zones indicate regions of 0 and π phase imprints, respectively.

Compared to other techniques, laser direct writing is flexible, easily handling and timesaving. In addition, due to the engravement on the fused silica, the multi-sector phase plate is low cost and has the capacity of generating high-intensity OAM modes, which is helpful in some applications. Here, we applied this rapid and easy operating solution of laser direct writing to produce binary multi-sector phase plates on fused silica. Employing the fabricated phase plates, we experimentally demonstrate that it functions well at generating OAM superposition states.

2. Design and fabrication

Mathematically, the OAM mode of light can be simply described by $\psi^l(r,\varphi) = A(\sqrt{2}r/w)^l \exp(-il\varphi)$ in the transverse plane, where φ is the angular coordinate, l defines the OAM mode number of photons, which can be any integer value, positive or negative, and w is the beam waist. In general, the selective projective measurement state consists of an inhomogeneous superposition of OAM modes. With alternate phase of 0 and π, binary multi-sector phase plates emerge as an extremely appropriate choice for generating OAM superposition states. The thickness difference is $\lambda/[2(n-n_0)]$ for a phase difference of π, where n is the refractive index of the material for the phase plate, n_0 is the refractive index of the surrounding medium, and λ is the wavelength of interest. Figure 1 illustrates four such phase patterns for the generation of OAM superposition states. The black and gray sectors represent zones with 0 and π phases, respectively. Considering a wavelength of 632.8 nm, the refractive index of the fused silica (HPFS 7980, Corning) is 1.457, and thus, the height difference of the sectors with a π phase difference is 692.3 nm.

As shown in Figure 2, the direct laser writing setup is equipped with a fs-laser (Pharos, Light Conversion), of which the central wavelength is 1025 nm. We employ a 280-fs-wide pulsed laser with a tunable repetition rate, tightly focused with a 20× objective lens (Mitutoyo Plan Apo NIR, Edmund). The fused silica sample is mounted on an xyz-stage, and precisely positioned at the focus by a pair of cylindrical lenses. When the writing laser focuses at the surface of the sample, a circular spot can be detected on the CCD. Otherwise, the spot on the CCD appears as an elliptical one, either horizontally or vertically oriented. Combined with the polarization beam splitter, the pulse energy is attenuated by rotating the half-wave plate. The image assembly is comprised of a green LED, beam delivery optics and CCD camera. It is essential to image the sample in real time to successfully manufacture the binary multi-sector phase plate. As the laser spot is moved by an xy-galvanometer, the phase pattern is rapidly imprinted on the surface of the fused silica. After a parametric study of the pulse energy, repetition rate, interval between two successive shots, and line distance of laser writing, the multi-sector phase plate is optimized with a thickness difference between two adjacent zones of ∼710 nm, which is close to 692.3 nm.

Femtosecond laser writing leads to a slightly rough surface on the fused silica binary multi-sector phase plate, which will lower the transmission. Generally, post-treatments such as acid etching are added to reduce the roughness, which may introduce impurities and increase the damage probability for applications at high power. Here, after writing with the femtosecond laser, the phase plates are irradiated and polished by a CO_2 laser operating at 10.6 μm. The quasi-CW (continuous wave) is chopped to a frequency of 5 kHz with a pulse width of 25 μs via an acousto-optic modulator. Figure 3 shows images of binary multi-sector phase plate

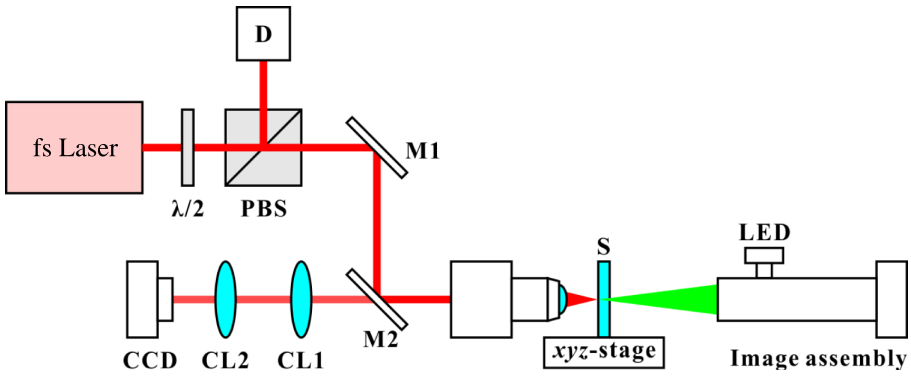

Figure 2. Setup of direct laser writing. $\lambda/2$: half-wave plate, PBS: polarization beam splitter, D: dump, M: mirror, CL: cylindrical lens, S: sample.

https://doi.org/10.1017/hpl.2018.1 Published online by Cambridge University Press

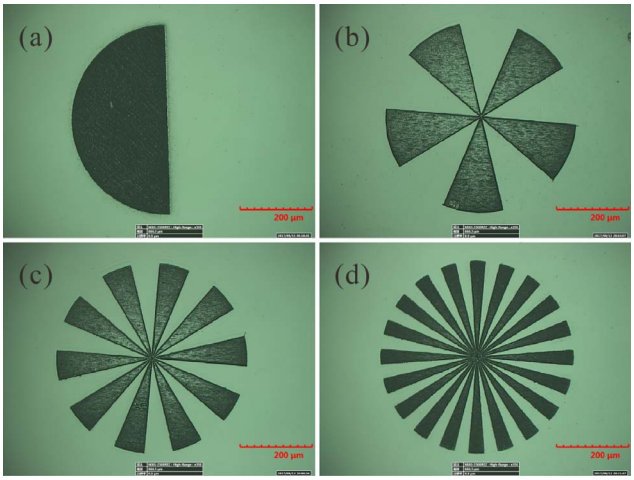

Figure 3. Images of fused silica binary multi-sector phase plate. (a) $|1\rangle + |-1\rangle$; (b) $|5\rangle + |-5\rangle$; (c) $|10\rangle + |-10\rangle$; (d) $|20\rangle + |-20\rangle$.

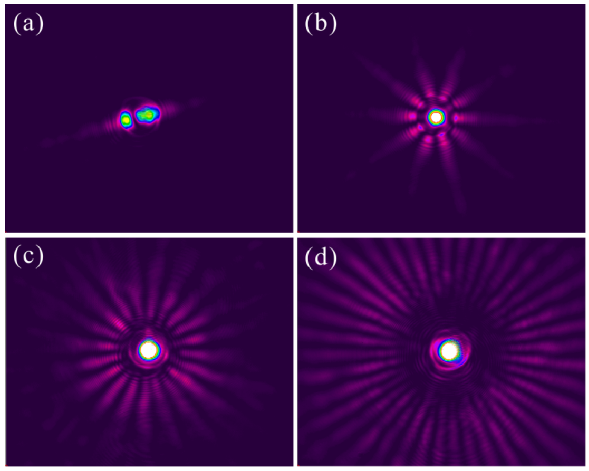

Figure 4. Measured intensity profiles of various states of the sample at a distance of 255 mm. The images have a resolution of 2753 × 2192 in pixel with a pixel size of 4.5 μm × 4.5 μm. (a) $|1\rangle + |-1\rangle$; (b) $|5\rangle + |-5\rangle$; (c) $|10\rangle + |-10\rangle$; (d) $|20\rangle + |-20\rangle$.

inscribed with different superposition states on the fused silica. The fabrication quality can be inferred from the good shape and sharp steps. The phase pattern has a diameter of 500 μm on the sample. Thus, a variety of patterns can be imprinted on a plate of common sizes, such as 20 mm × 20 mm, which offers the convenience to alter the phase patterns for different cases simply by choosing the position of interest on the plate.

3. Characterization and discussion

The fabricated phase plates were characterized with a Gaussian beam emitted by a He–Ne laser (HNL008L, Thorlabs). The beam was reshaped by a lens of focal length $f = 150$ mm. We mounted the fabricated phase plate on a linear motion stage to adjust the z-position, herein the focus position and Gaussian spot size. A CCD (LT665, Ophir) located at a distance of 225 mm from the plates was used to capture the intensity profile, as shown in Figure 4. In accordance with the expected patterns, the Gaussian spot, with a diameter of 238 μm at $1/e^2$, is separated into 2, 10, 20 and 40 petals passing through the binary multi-sector phase plates for the OAM superposition states of $|1\rangle + |-1\rangle$, $|5\rangle + |-5\rangle$, $|10\rangle + |-10\rangle$ and $|20\rangle + |-20\rangle$, respectively. In addition, the entire light spot and dark zone at the center increase with the order of OAM modes. The intensity of the beam center for the superposition states of $|\psi_{\pm}(l)\rangle$ should always be zero. However, for $|l| > 5$, a bright center can be observed for the generated beam, which results from the imperfects of the fabricated phase plates.

The imperfects mainly include the overwritten center of the phase plate, the error of the phase difference, and the transmissivity difference among the sectors. Taking mode of $|5\rangle + |-5\rangle$ for example, we separately analyze the effects of the three facets on the generated beam profiles, respectively. First, because the center of the phase plate is overwritten, the phase of this area is not different but nearly same between adjacent sectors. As shown in Figure 5, the intensity profiles vary with different overwritten areas. The waist radius of input Gaussian beam is 2 mm. The contrast of the petal-like structure and central spot increases gradually with the decrease of the radius ratio between the overwritten area and input Gaussian beam. Only when the ratio is less than 0.1, there is no obvious effect on the generated beam profile. Second, when the error of the phase difference, or the height difference engraved by laser, between adjacent sectors is increasing, the contrast of the petal-like structure and central spot is lowering as well, as shown in Figure 6. When the error is less than 0.1π, there is almost no obvious effect on the generated beam profile. Third, the transmissivity between adjacent sectors is also slightly different as the roughness between them varies after laser writing. Figure 7 displays the calculated intensity profiles under different transmissivity ratios between adjacent sectors. The poorer the uniformity of transmissivity is, the lower the contrast of the petal-like structure and central spot is. Nevertheless, there is no need to take the impact on the intensity profile into account when the transmissivity ratios are higher than 0.8. Based on the theoretical calculations, we carefully control the overwritten area and height difference and fabricate a phase plate with a diameter of 4 mm to generate mode of $|5\rangle + |-5\rangle$. The Gaussian beam emitted from the He–Ne laser is expanded and collimated. It has been found that the quality of the generated beams is slightly improved, as shown in Figure 8. But due to the roughness remains different, the transmissivity between adjacent sectors is still inhomogeneous. Thus, the central spot remains brighter. The transmissivity inhomogeneity can be improved by more precise control of the energy deposition during the process of laser writing and laser polishing.

https://doi.org/10.1017/hpl.2018.1 Published online by Cambridge University Press

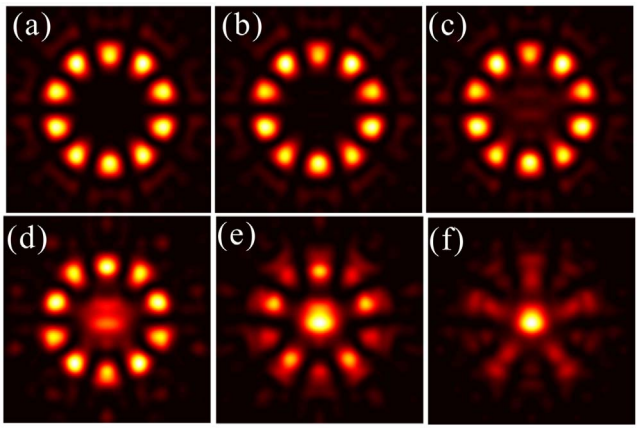

Figure 5. Calculated intensity profiles of $|5\rangle + |-5\rangle$ under different radii of the overwritten area. The waist radius of the input Gaussian beam is 2 mm. (a) 100 μm; (b) 200 μm; (c) 400 μm; (d) 600 μm; (e) 800 μm; (f) 1000 μm.

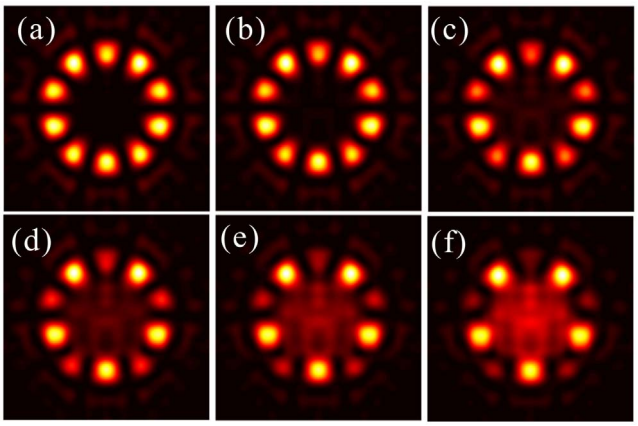

Figure 6. Calculated intensity profiles of $|5\rangle + |-5\rangle$ under different errors of the phase difference. (a) 0; (b) 0.1π (c) 0.2π; (d) 0.3π; (e) 0.4π; (f) 0.5π.

This type of multi-sector phase plate can be used to measure OAM entanglement from a spontaneous parametric down-conversion process. Using two identical multi-sector phase plates, specific OAM components of entanglement are able to be selectively filtered by the projection states. The projection state is generally an extended superposition of OAM modes, which depends on the phase distribution and orientation of the plates[33]. Specially designing the sector angles of the binary multi-sector phase plates, the Shannon dimensionality D of an entanglement state can be maximized[32]. For example, with an optimized 10-sector phase plate, D can be achieved as high as 50[32]. Fabrication of such an optimized phase plate with the proposed method is very simple as long as the sector angles are figured out, though we did not manufacture these special phase patterns. Generally, the laser-induced damage threshold of fused silica is higher than 4 J/cm^2 at the pulse duration in nanosecond regime[41]. The multi-sector phase plate fabricated from the fused silica can perform well under high intensity, which adds the number of applications and is very helpful to some existing applications, such as improving the signal intensity of remote sensing.

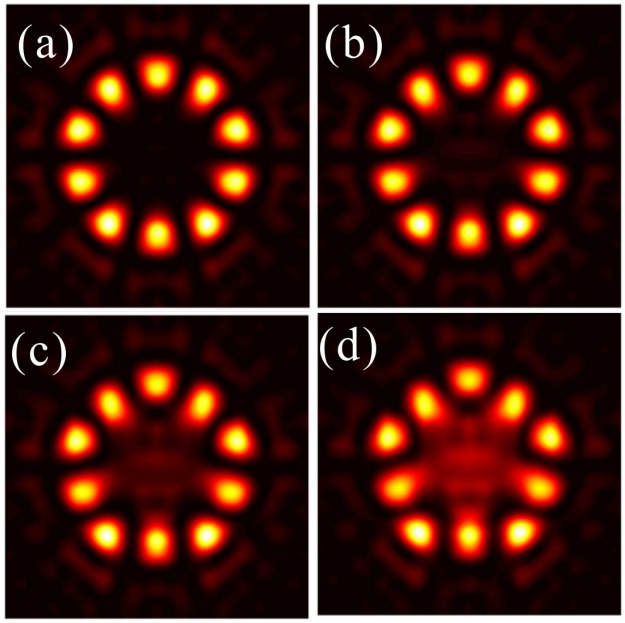

Figure 7. Calculated intensity profiles of $|5\rangle + |-5\rangle$ under different transmissivity ratios between adjacent sectors. (a) 0.8; (b) 0.6; (c) 0.4; (d) 0.2.

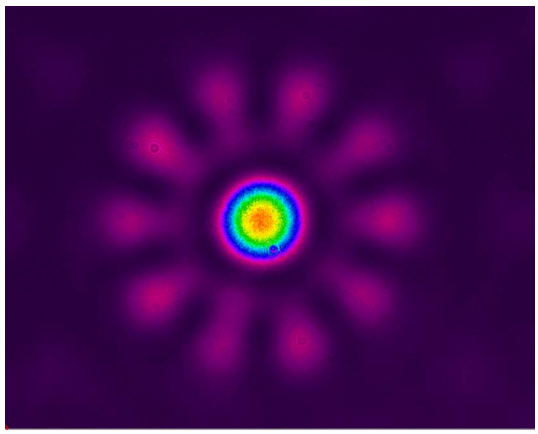

Figure 8. Measured intensity profile of the superposition modes of $|5\rangle + |-5\rangle$ at a distance of 9 m. The image has a resolution of 2753 × 2192 in pixel with a pixel size of 4.5 μm × 4.5 μm.

4. Conclusion

Binary multi-sector phase plates play an important role in entanglement measurement as OAM state analyzers. By combining fast femtosecond laser direct writing with CO_2 laser polishing, the phase plates for generating OAM superposition states are successfully manufactured on fused

https://doi.org/10.1017/hpl.2018.1 Published online by Cambridge University Press

silica. These high-performance binary multi-sector phase plates can be fabricated with smaller sizes if necessary, and they can be conveniently integrated with other micro-optics. In addition, the intensity profiles agree well with the expected pattern, though a bright center is observed. By eliminating the transmissivity inhomogeneity between adjacent sectors with a more precise control of the energy deposition during the manufacturing procedure, this method will be very competitive in the production of phase plates, for not only binary plates but also continuous plates.

Acknowledgements

The authors thank the financial support by the Youth Innovation Promotion Association, Chinese Academy of Sciences.

References

1. L. Allen, M. W. Beijersbergen, R. J. Spreeuw, and J. P. Woerdman, Phys. Rev. A **45**, 8185 (1992).
2. N. B. Simpson, L. Allen, and M. J. Padgett, J. Modern Opt. **43**, 2485 (1996).
3. M. E. J. Friese, H. Rubinsztein-Dunlop, J. Gold, P. Hagberg, and D. Hanstorp, Appl. Phys. Lett. **78**, 547 (2001).
4. K. Ladavac and D. G. Grier, Opt. Express **12**, 1144 (2004).
5. D. Luo, C. F. Kuang, X. Hao, and X. Liu, Opt. Lasers Eng. **50**, 944 (2012).
6. C. Rosales-Guzman, N. Hermosa, A. Belmonte, and J. P. Torres, Opt. Lett. **39**, 5415 (2014).
7. M. P. J. Lavery, F. C. Speirits, S. M. Barnett, and M. J. Padgett, Science **34**, 537 (2013).
8. C. Rosales-Guzman, N. Hermosa, A. Belmonte, and J. P. Torres, Sci. Rep. **3**, 2815 (2013).
9. M. P. J. Lavery, S. M. Barnett, F. C. Speirits, and M. J. Padgett, Optica **1**, 1 (2014).
10. D. B. Phillips, M. P. Lee, F. C. Speirits, S. M. Barnett, S. H. Simpson, M. P. J. Lavery, M. J. Padgett, and G. M. Gibson, Phys. Rev. A **90** (2014).
11. H. Martin, Astrophys. J. **597**, 1266 (2003).
12. G. Milione, T. Wang, J. Han, and L. Bai, Chin. Opt. Lett. **15**, 030012 (2017).
13. J. Wang, J.-Y. Yang, I. M. Fazal, N. Ahmed, Y. Yan, H. Huang, Y. Ren, Y. Yue, S. Dolinar, M. Tur, and A. E. Willner, Nat. Photon. **6**, 488 (2012).
14. M. Mohammad, S. M.-L. Omar, N. O. S. Malcolm, R. Brandon, M. Mehul, P. J. L. Martin, J. P. Miles, J. G. Daniel, and W. B. Robert, New J. Phys. **17**, 033033 (2015).
15. R. Fickler, R. Lapkiewicz, W. N. Plick, M. Krenn, C. Schaeff, S. Ramelow, and A. Zeilinger, Science **338**, 640 (2012).
16. A. Mair, A. Vaziri, G. Weihs, and A. Zeilinger, Nature **412**, 313 (2001).
17. J. T. Barreiro, T.-C. Wei, and P. G. Kwiat, Nat. Phys. **4**, 282 (2008).
18. N. Lütkenhaus, Phys. Rev. A **54**, 97 (1996).
19. L. Zhang, C. Silberhorn, and I. A. Walmsley, Phys. Rev. Lett. **100**, 110504 (2008).
20. B. P. Lanyon, M. Barbieri, M. P. Almeida, T. Jennewein, T. C. Ralph, K. J. Resch, G. J. Pryde, J. L. O'Brien, A. Gilchrist, and A. G. White, Nat. Phys. **5**, 134 (2009).
21. A. Forbes, A. Dudley, and M. McLaren, Adv. Opt. Photonics **8**, 200 (2016).
22. E. Yao, S. Franke-Arnold, J. Courtial, M. J. Padgett, and S. M. Barnett, Opt. Express **14**, 13089 (2006).
23. S. Zhou, S. Wang, J. Chen, G. Rui, and Q. Zhan, Photon. Res. **4**, B35 (2016).
24. Y. Chen, Z. X. Fang, Y. X. Ren, L. Gong, and R. D. Lu, Appl. Opt. **54**, 8030 (2015).
25. L. Gong, Y. Ren, W. Liu, M. Wang, M. Zhong, Z. Wang, and Y. Li, J. Appl. Phys. **116**, 183105 (2014).
26. S. A. Goorden, J. Bertolotti, and A. P. Mosk, Opt. Express **22**, 17999 (2014).
27. K. J. Mitchell, S. Turtaev, M. J. Padgett, T. Cizmar, and D. B. Phillips, Opt. Express **24**, 29269 (2016).
28. C. Zhang, C. Min, and X. C. Yuan, Opt. Commun. **381**, 292 (2016).
29. M. Mirhosseini, O. S. M. na Loaiza, C. Chen, B. Rodenburg, M. Malik, and R. W. Boyd, Opt. Express **21**, 30204 (2013).
30. G. Campbell, B. Hage, B. Buchler, and P. K. Lam, Appl. Opt. **51**, 873 (2012).
31. Z. Liu, Y. Liu, Y. Ke, Y. Liu, W. Shu, H. Luo, and S. Wen, Photon. Res. **5**, 15 (2017).
32. B. J. Pors, F. Miatto, G. W. Hooft, E. R. Eliel, and J. P. Woerdman, J. Opt. **13**, 064008 (2011).
33. J. B. Pors, S. S. Oemrawsingh, A. Aiello, M. P. van Exter, E. R. Eliel, G. W. 't Hooft, and J. P. Woerdman, Phys. Rev. Lett. **101**, 120502 (2008).
34. S. S. Oemrawsingh, J. A. van Houwelingen, E. R. Eliel, J. P. Woerdman, E. J. Verstegen, J. G. Kloosterboer, and G. W. 't Hooft, Appl. Opt. **43**, 688 (2004).
35. G. Ruffato, M. Massari, M. Carli, and F. Romanato, Opt. Eng. **54** (2015).
36. K. Sueda, G. Miyaji, N. Miyanaga, and M. Nakatsuka, Opt. Express **12**, 3548 (2004).
37. G. Knoner, S. Parkin, T. A. Nieminen, V. L. Loke, N. R. Heckenberg, and H. Rubinsztein-Dunlop, Opt. Express **15**, 5521 (2007).
38. E. Brasselet, M. Malinauskas, A. Zukauskas, and S. Juodkazis, Appl. Phys. Lett. **97** (2010).
39. X. Wang, A. A. Kuchmizhak, E. Brasselet, and S. Juodkazis, Appl. Phys. Lett. **110**, 181101 (2017).
40. A. Žukauskas, M. Malinauskas, and E. Brasselet, Appl. Phys. Lett. **103**, 181122 (2013).
41. R. A. Negres, M. A. Norton, D. A. Cross, and C. W. Carr, Opt. Express **18**, 19966 (2010).

https://doi.org/10.1017/hpl.2018.1 Published online by Cambridge University Press